Proceedings of the ASME 2024
International Mechanical Engineering Congress and Exposition
IMECE2024
November 17-21, 2024, Portland, Oregon

IMECE2024-145828

BIOROBOTIC ACTUATOR SELECTION SPACE MAPPING

Pavlos Hanna
University of Technology Sydney
Sydney, Australia

Marc Carmichael
University of Technology Sydney
Sydney, Australia

Lee Clemon
University of Illinois
Illinois, IL

ABSTRACT

Actuator selection is critical in the design of human compatible robotics, such as prosthetics, exoskeletons, and humanoids. Each has its own set of parameters, from output specifications to package sizing and applicable environmental conditions. A multitude of design factors must be considered in selection, some are dictated by performance relations, while other engineering decisions are latent and unobserved. In biorobotic design, weight is often a key trade-off parameter with actuator performance. We analyze a database of over 1900 motors that are of relevant size for biorobotic designs to identify underlying trends that affect selection options. Selected motors range from 0.000013Nm to 3.66Nm in torque and 0.0016kg to 5.67kg in weight. We then generate Ashby-style charts to evaluate trends across motor selection dimensions. We find a wide disparity between manufacturers and where their actuators are specialized. The results provide a means for rapidly narrowing the selection space for designers, which is shown through an example application and reduces design time and improves the actuator selection.

Keywords: actuators, cobots, design optimization, exoskeletons, generative design, robotics.

1. INTRODUCTION

Actuators are used in many applications particularly in robotics and robotic related applications. Finding actuators that exactly match the requirements is generally not possible and usually there is a compromise that is made.

Use of actuators in prosthetics, exoskeletons, exosuits and humanoids are particularly relevant as these are primarily driven by one of two methods; 'electromechanical actuation or soft inflatable materials' [1-10]. This use of robots alongside humans, cobots, belongs to the overarching field of service robotics and is known to be 'one of the most challenging parts in robotics' [11]. One thing that is prevalent in all these is that they 'must transmit a controlled amount of torque in a way that is safe, comfortable and effective' [12-19].

Due to these devices being carried by a human user, the device needing to fit within a specific form factor, and producing specific output characteristics, selecting the 'smallest' actuator that suits the system specifications has substantial follow on effects for full system design [20]. As such, this paper looks at motors that are aptly sized for use in humanoid scale robotic applications. There is a vast number of available actuators from various suppliers, so selecting a suitable actuator is a complicated and time-consuming task. More so, selecting the most ideal actuator is even more challenging as it depends on designer knowledge and available search time.

Currently much research exists on how to select an actuator for a particular use case, and many papers have utilized this to create assistive robots that function well. On the design of robotic hands alone, Birglen and Gosselin [21, 22] discuss over 25 different designs by others created from the 1960s through the 2000s. These designs use a host of actuation methods including hydraulic, mechanical, pneumatic and tendon-based drives. However, these processes are a manual task which require the designer knowing the target and having experience in correctly defining what is needed. As such, these are lengthy processes and need to be conducted from the beginning each time a new set of requirements are proposed.

This paper aims to map a database for searching the wide range of actuators within a range of actuators that are useable in the biorobotic field. This dataset is organized into a design tool that plots the properties of each actuator on varying graphs and creates various Ashby charts to rapidly narrow the selection space for designers. These charts provide insight into trends and can be utilized directly as look up charts to speed up the initial selection process.

The processes and research done here can be applied to the selection process of actuators in any application by varying the actuator parameter requirements that are used within the dataset. An example of this would be the selection of an actuator for a drone motor. Based on data from a range of drone design papers [23-27] rotor speeds of 900-20000 rpm are needed. A database

including motors that achieve these speeds could be created, and then Ashby charts based on vendor cost or some other parameter produced for the relevant design requirements in drone motor selection.

2. METHODOLOGY

To select only actuators that are aptly sized for use in humanoid scale robotic applications, we need to define a parameter to constrain the search space by. This is done by using data on human strength at each of the major joints; ankle, knee, hip, wrist, elbow and shoulder in the primary plane of movement.

Torque and speed are the values that we are interested in. From tests on 1000 children and adults conducted by the American Academy of Neurology [28], we get the maximum force values at each of the human joints along with angle of rotation and joint speed values.

These force values are coupled with the distances that the forces were measured at from the joint to give the torque values. From Bohannon (1997) [29] we find the location of where the forces are measured. Looking at the anthropometric dimensions of these locations to the joints using data from the Anthropometric Survey of U.S. Personnel conducted in 1989 by Gordon Claire C of 75000 personnel [30] we find the moment arm lengths and hence the torque produced can be calculated.

This resultant torque produced at these joints in their strongest plane of articulation is outlined in Table 1 below. Mathematical models exist [31-34] which allow us to calculate the required torque to account for the weight of the exoskeleton and losses within the system.

TABLE 1: TORQUE VALUES FOR HUMAN JOINTS

Joint	Average torque[1] (Nm)	Max torque[2] (Nm)
Ankle	66.4	118.5
Knee	202.1	400.0
Hip	109.0	238.8
Wrist	12.9	16.1
Elbow	72.9	156.0
Shoulder	118.9	143.3

[1] Largest average torque of 20-59-year-old age group.
[2] Max torque computed from largest force and limb length.

Based on an extension on the work done by Hanna (2021) [35] which looked at the elbow joint and determined the suitable motor gearbox combinations needed, we apply the same method to the knee joint as it is the highest torque demanding joint in the body. In the paper, for the elbow joint, it was found that the max torque needed was under 1.42Nm once coupled with an appropriate gearbox. At 400Nm for the knee joint compared to the elbows 156Nm peak torque, we can calculate that an equivalent value for the knee joint actuator is 3.65Nm.

A total of 1968 commercially available direct current electric motors were collected up to this torque value and are used as the dataset within this paper.

Catalogues were collected from the public web pages of the motor manufacturers and suppliers. Motor manufacturers that have been included in this study consist of, MOOG, Maxon, EBM-Papst, Pololu, Allied Motion, Portescap and Faulhaber. This was based on the catalogues being publicly available and inclusive of sufficient information of parameter values needed for this study. See Table 2 below for a breakdown of the proportions of motors based on manufacturer.

Alongside the motor manufacturer and the motor type, brushed or brushless, the parameters of torque, weight, and speed were recorded. Current and voltage were also collected to be used to compute the power for the motors if not stated. This dataset has been made publicly available and can be found via contacting the authors.

A database was populated with these parameters and then filtered to remove any motors which were outside the ranges that are of interest. Selected motors ranged up to 3.65Nm in torque and resulted in an upper limit of 5.67kg in weight.

The data was categorized by manufacturer and if brushed or brushless. It was then plotted on both normal and logarithmically scaled axis, and convex hull boundaries were created around each category of datapoints.

In most applications, torque is the main parameter that needs to be matched to requirements. Following torque, weight, power and speed take varying priority depending on the specific application. From Hanna (2021) [35], the relationships we are interested in are the pairs of torque vs speed, weight and power, weight vs speed, power vs weight and speed.

Visual analysis of each plot comparing the various manufacturers and motor types were conducted along with analysis of the same manufacturer across various plots were done to see if any new insight could be made about which plot type would be most useful to use for a generative design process.

3. RESULTS

The output from the database after the filtering is applied is summarized in Table 1 below. The color refers to the color that is used in the plots. All plots follow the same color scheme for the legend.

TABLE 2: OVERVIEW OF PLOTS

Color	Manufacturer	Motor type	Number of motors	Percentage of database
Green	Maxon	Brushed	943	47.92%
Pink	Portescap	Brushless	270	13.72%
Maroon	Maxon	Brushless	245	12.45%
Red	MOOG	Brushless	207	10.52%
Yellow	Faulhaber	Brushed	167	8.49%
Cyan	Pololu	Brushed	59	3.00%
Purple	MOOG	Brushed	43	2.18%
Black	Allied Motion	Brushless	18	0.91%
Blue	EBM-Papst	Brushed	12	0.61%
Orange	Faulhaber	Brushless	4	0.20%

Certain trends are visible in the various plots; some are general trends, and some are specific to each individual motor manufacturer. Generally, brushless motors cover a larger spread of datapoints and generally have better specifications over brushed motors.

Other general trends are;

- As speed increases torque decreases; indicative that motors are designed for either torque or speed (Fig 1)
- As weight increases torque increases; indicative that larger motors can produce more torque (Fig 2)
- As power increases torque increases; indicative that more power results in higher output torque (Fig 3)
- As speed increases weight decreases; indicative that heavier, bigger motors are designed for torque (Fig 4)
- As weight increases power increases; indicative that motors need to be larger to handle higher power (Fig 5)
- As speed increases power decreases; indicative that motors that are designed for speed are not high torque, hence requiring less power (Fig 6)

This is in alignment with the basic theoretical fundamental equations behind actuators as can be seen from the two equations for torque on a coil and speed below.

$$T = N*B*I*A \quad (1)$$

$$T = (I*V*60) / (2*\pi*\omega) \quad (2)$$

Based on the first equation, torque is directly proportional to the number of coils (N) which increasing will increase mass, magnetic field strength (B) which increasing requires a bigger stator magnet, current (I) which increasing increases power and coil area (A) which increasing requires a larger motor hence increasing weight.

From the second equation where input power (I*V) is a constant, we see that torque is inversely proportional to speed (ω).

For this reason, some manufacturers focus on higher torque (e.g. MOOG brushless) while others focus on higher speed (e.g. Maxon brushless). Portescap brushless focuses on higher torque for lower weights and lower power, while Faulhaber brushless focuses on high speeds for low weight and power.

Additional interesting trends can be seen when comparing manufacturers and motor type across plots. Considering Fig 2 and Fig 3 the main difference that is seen is that some of the convex hulls shift location while others do not. Particularly, MOOG brushed is seen to shift location, while most others are fairly unchanged between the two plots. This can be linked and attributed to Fig 5, where the MOOG brushed is the only motor that spans a wide range horizontally without much change vertically. This imbalance translates into a more vertical plot in the torque vs power plot and a more horizontal plot in the torque vs weight due to the relationships between these parameters in the above equations. A similar case is in the weight vs speed plot where only a very small range of speeds are observed for the MOOG brushed motor within this category.

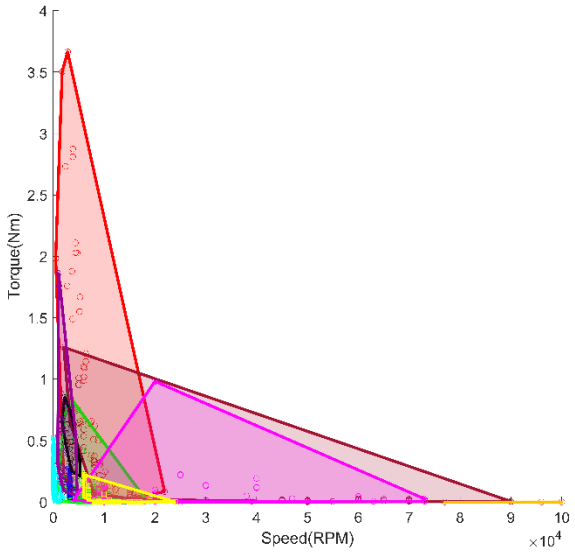

FIGURE 1: TORQUE VS SPEED

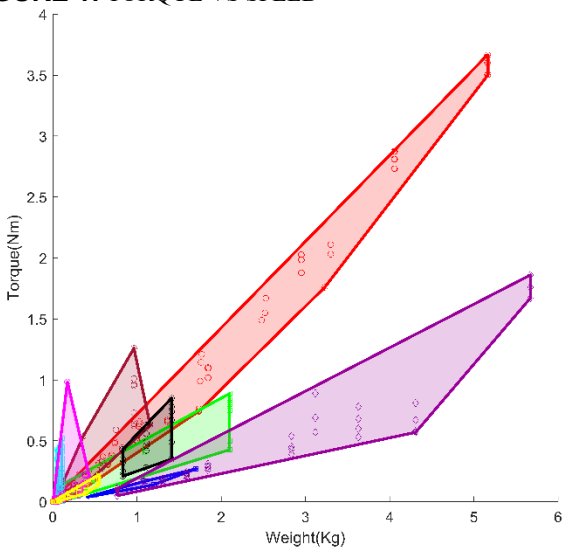

FIGURE 2: TORQUE VS WEIGHT

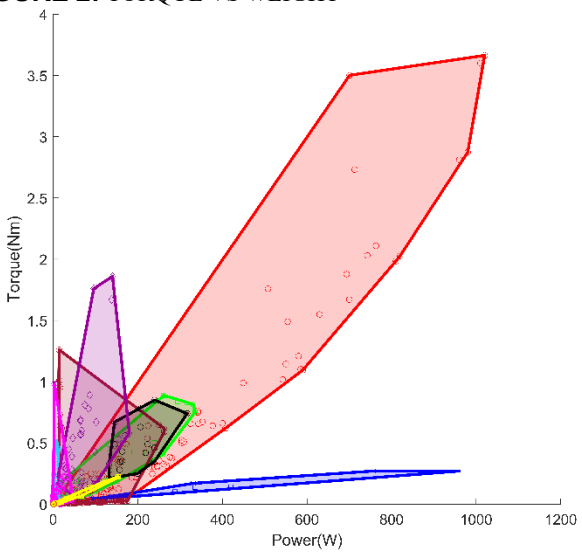

FIGURE 3: TORQUE VS POWER

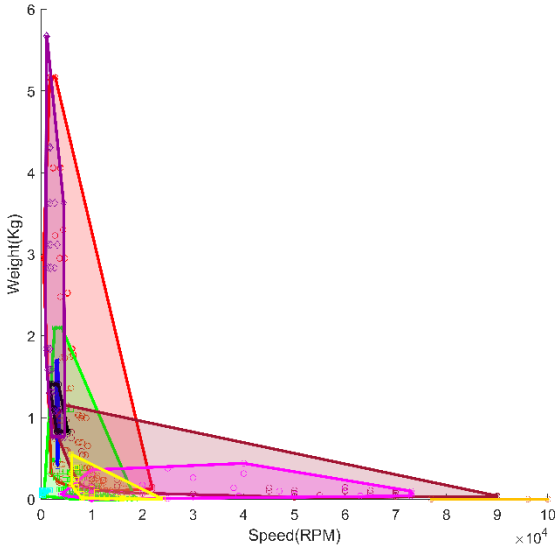

FIGURE 4: WEIGHT VS SPEED

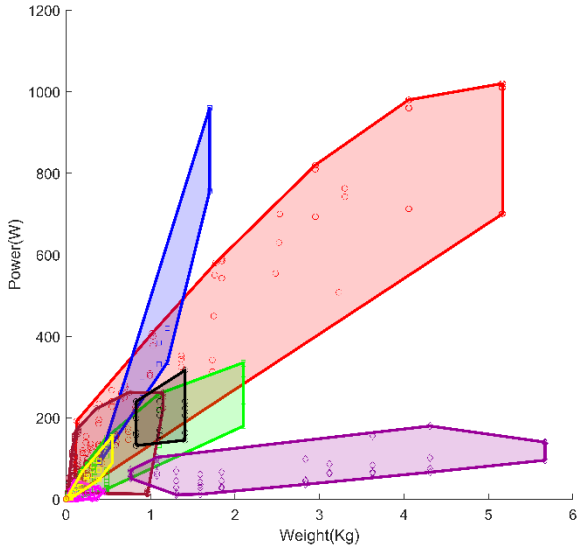

FIGURE 5: POWER VS WEIGHT

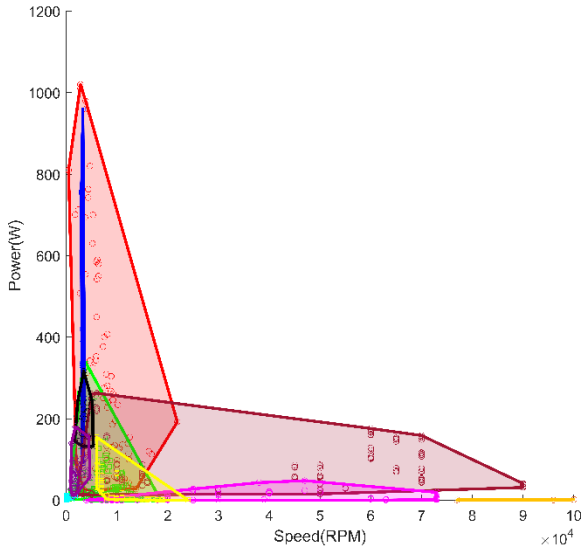

FIGURE 6: POWER VS SPEED

Due to a large proportion of the datapoints existing within a small range around the origin, and others being further away, these linear plots lose a lot of information. For this reason, logarithmically scaled plots are also created. These scaled plots are found to show more disparity between each of the data sets and provides a more useful chart, particularly for the plots that include speed as a parameter which is better suited for a generative design tool.

The size of the regions on the logarithmic plots also give indication to the range across orders of magnitude for each manufacturer. For example, in Fig 7, Allied Motion brushless, EBM-Papst brushed and Faulhaber brushless occupy small widths on the graph indicating that they are specialized around motors at those specific speeds. Compare that to Pololu brushed or Portescap brushless, where they span wider ranges and hence produce motors at a larger range of speeds.

Due to the clustered nature of the regions on the linear plots as seen in Fig 1 above, we lose the information that Pololu brushed spans a wider range of speeds than is depicted in the linear plots. This is where the visual analysis of the plots further shows that the logarithmic plots are better suited to be used as a design tool.

The figures of torque vs weight and power (Fig 8 and Fig 9) still maintain the linear relationship between these parameters as expected.

Unlike with the linear plots for the comparison between the torque vs weight and torque vs power plots, there is no significant difference in location of any particular motor group. The convex hulls relative location of each manufacturer to one another remains relatively consistent within these plots. This difference is also represented in Fig 11 as all the regions generally match what is displayed in Fig 8 and Fig 9. This correspondence between the normal and logarithmic plots is expected and indicates that graphs can be cross referenced and used in subsets as 3 plots can be used to infer the remaining plots, e.g. Using Fig 7 and Fig 8 to find the data on Fig 10.

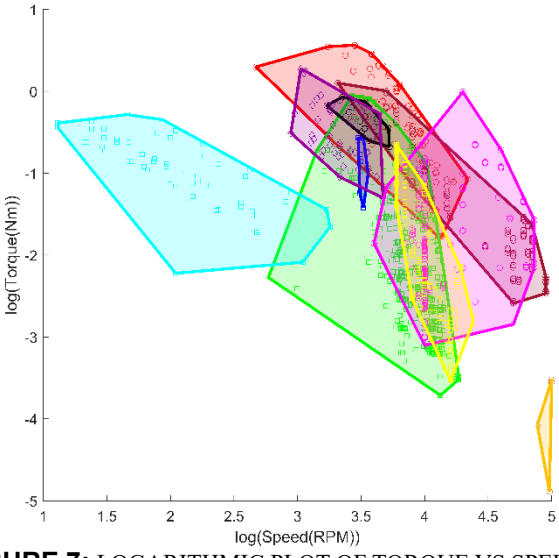

FIGURE 7: LOGARITHMIC PLOT OF TORQUE VS SPEED

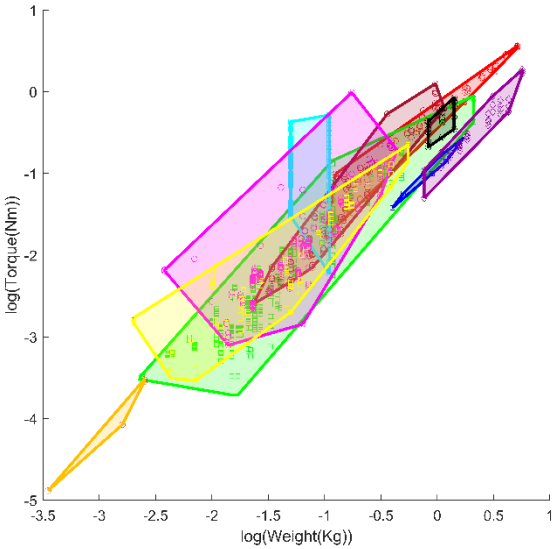

FIGURE 8: LOGARITHMIC PLOT OF TORQUE VS WEIGHT

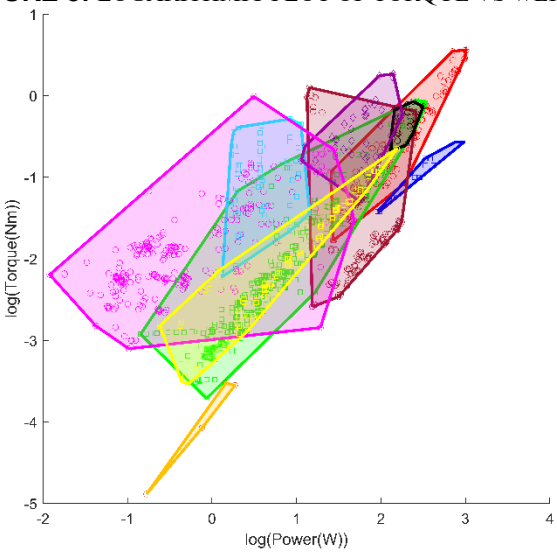

FIGURE 9: LOGARITHMIC PLOT OF TORQUE VS POWER

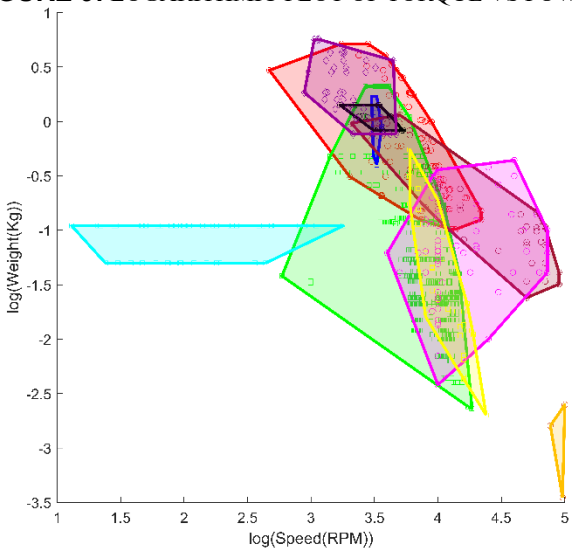

FIGURE 10: LOGARITHMIC PLOT OF WEIGHT VS SPEED

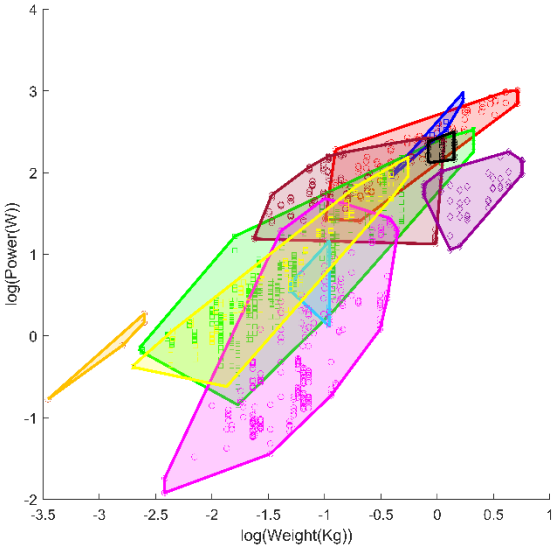

FIGURE 11: LOGARITHMIC PLOT OF POWER VS WEIGHT

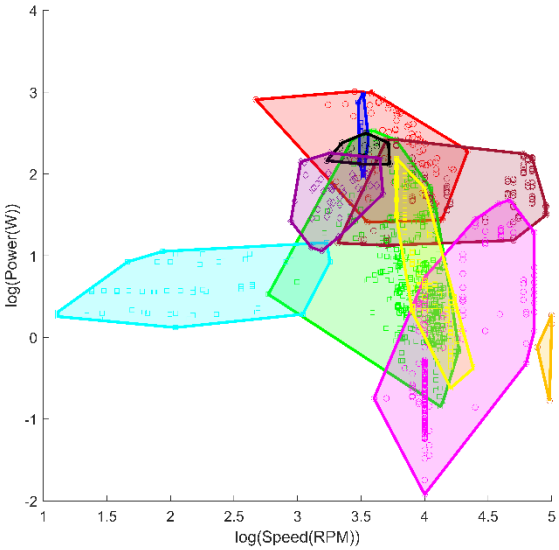

FIGURE 12: LOGARITHMIC PLOT OF POWER VS SPEED

The logarithmic plots also show the regions in a way that is more representative between polygon size and the proportion of motors from that manufacturer. This can be seen by considering how the datapoints within the convex hulls in the logarithmic plots spread over most of the enclosed area, while in the linear plots there are large sections within the convex hulls without datapoints present. The logarithmic plots also spread the regions out allowing for better visual observation of each convex hull boundary.

4. EXAMPLE APPLICATION

Analyzing the same example of the elbow joint as Hanna (2021) [35], we see that we are after a motor with approximate values as following; torque greater than 0.91Nm, speed between 3300-8000rpm, a power maximum of 345W and weight between 0.09kg and 1.3kg.

Going through the logarithmic based plots and marking out the bounds, we get the figures 13-18 below.

From each of the plots, the motor manufacturers that achieve the target parameters are easily found.

Figure 13 below for torque vs speed shows only Maxon and MOOG brushless motors as suitable.

Figure 14 below for torque vs weight shows Maxon, MOOG and Portescap brushless motors as suitable.

Figure 15 below for torque vs power shows Maxon, MOOG, Portescap brushless and MOOG brushed motors as suitable.

Figure 16 below for weight vs speed shows all except Pololu brushed and Faulhaber brushless as suitable.

Figure 17 below for power vs weight shows only Faulhaber brushless as not suitable.

Figure 18 below for power vs speed shows all except Pololu brushed and Faulhaber brushless as suitable.

Considering all these regions, the only manufacturers which achieve all required parameters within some region of their convex hull are Maxon and MOOG brushless motors. In saying this however, closer inspection shows that for MOOG in both figures 14 and 15, there are no datapoints within the bounded region within the convex hull. This stipulates that although the database does not contain an actuator that matches the required parameters, there is a more probable likely hood that the manufacturer could have a motor that is suitable that just has not been included in the database that was used to create the plots.

This leaves Maxon brushless as the sole manufacturer and motor type that achieves all requirements. Going through the database considering only Maxon brushless motors, there are three motors with the following specifications in Table 3 below that achieve the desired parameters. They are the EC 90 flat model numbers 500269, 500267 and 607950.

TABLE 3: PARAMATER VALUES FOR SUITABLE MOTORS

Model	Torque (Nm)	Weight (kg)	Power (W)	Speed (RPM)
500269	1.01	0.964	14.94	5000
500267	0.964	0.964	13.344	5000
607950	0.953	0.964	16.704	5000

Considering the motors that were selected by Hanna (2021) [35], which are stated in Table 4 below, we see that although, as explained in that paper, having larger torque and speed values than required still allows for a solved model, our selected motors are actually within the search range, and although they weigh more, they require less power. This indicates that they are a better fit for the application.

TABLE 4: SPECIFICATIONS OF CHOSEN MOTORS BY HANNA

Model [1]	Torque (Nm)	Weight (kg)	Power (W)	Speed (RPM)
BN12-13AF01	2.4	0.102	27.12	13027
BN12-13AF03	2.4	0.102	27.72	13753
BN12-13AF02	2.4	0.102	27.12	12736

[1] MOOG Silencer brushless motor model numbers.

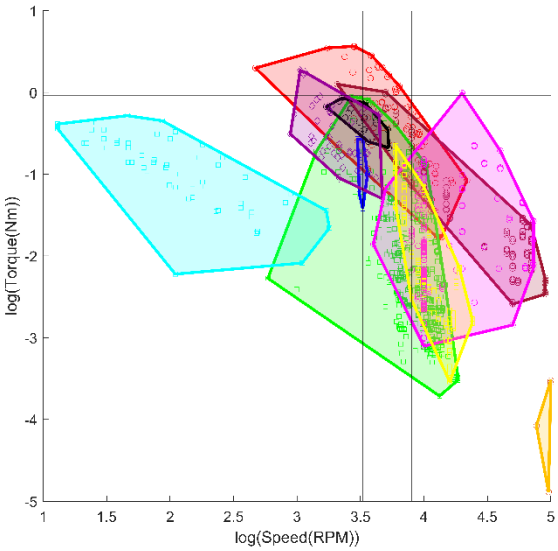

FIGURE 13: LOGARITHMIC PLOT OF TORQUE VS SPEED

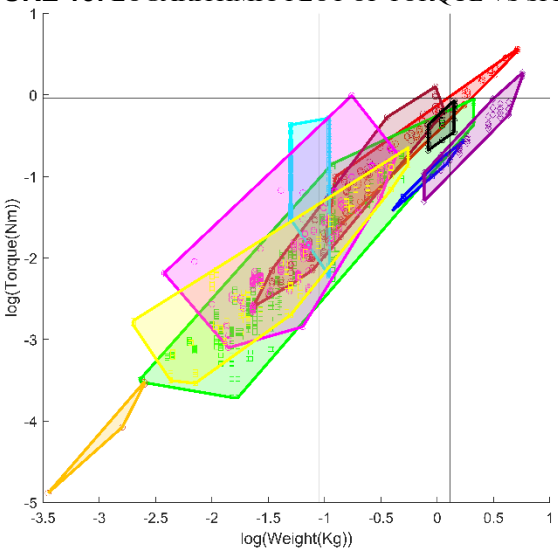

FIGURE 14: LOGARITHMIC PLOT OF TORQUE VS WEIGHT

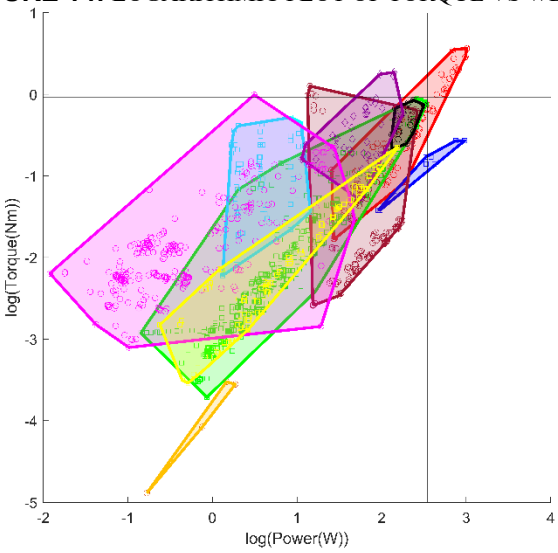

FIGURE 15: LOGARITHMIC PLOT OF TORQUE VS POWER

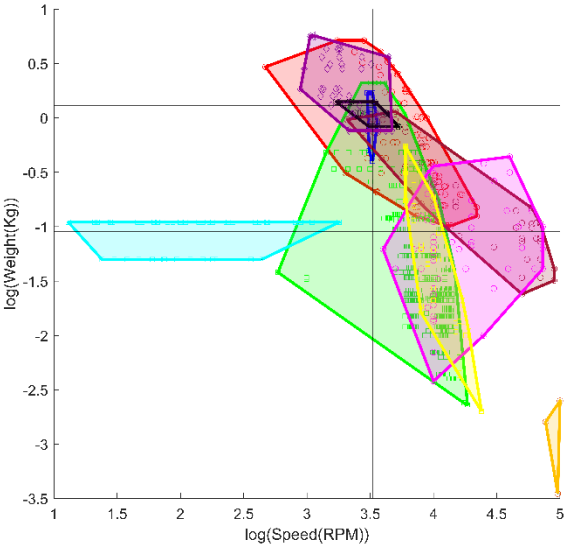

FIGURE 16: LOGARITHMIC PLOT OF WEIGHT VS SPEED

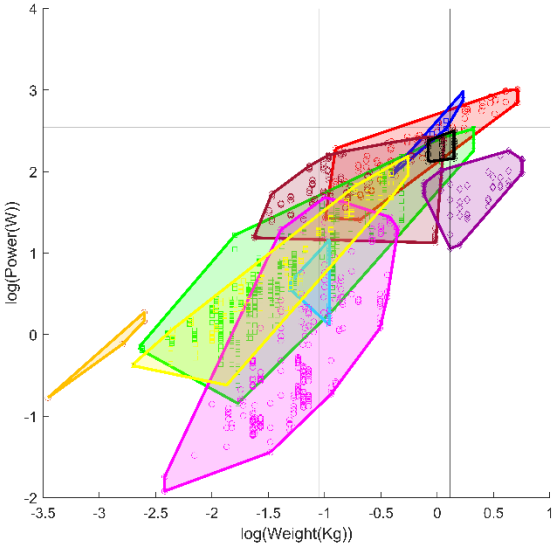

FIGURE 17: LOGARITHMIC PLOT OF POWER VS WEIGHT

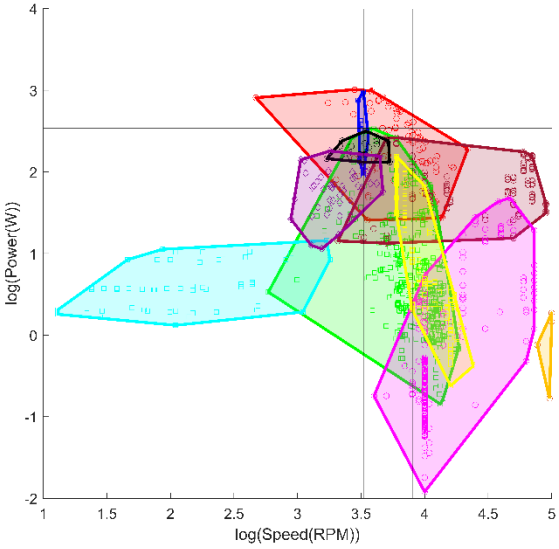

FIGURE 18: LOGARITHMIC PLOT OF POWER VS SPEED

5. DISCUSSION

These plots help determine if a suitable actuator possibly exists for a given application. They allow for a shortened design process by replacing a normally guided random actuator selection process with a systematic approach. The implications of this is that for biorobotic use cases, the ability to efficiently select actuators could mean that each prosthetic or exoskeleton could potentially be designed and tailored to the individual.

5.1 Ashby Charts

Considering the fundamental equations that govern electric motors as aforementioned, conditional to plots not involving weight, it can be inferred that any point within each convex hull is a set of parameters to which a motor could be manufactured. If the convex hull has a point that is furthest to the top right of the plot, then it is guaranteed that a motor could be made that would achieve any pair of parameters within that convex hull, more so, any actuator with parameters lying within a rectangle from the origin to that point. This is the case as for any pairwise parameters, if a motor exists which exceeds the demand for those two parameters, it can be used in place where any set of parameters lower than it are needed for either axis. For example, if a motor exists which produces a torque of 3Nm and a speed of 1000rpm, then any application which requires an actuator to run less than 1000rpm and produce torque less than 3Nm, that particular actuator could be used for and not be run to its full capacity. This in turn means that the actuator could be modified by reducing the number of coils or changing its size for example, to result in a new actuator which runs ideally at those required parameters. For the plots that include weight as a parameter, similar reasoning works for the furthest left point.

Although these plots are useful in determining if an actuator exists with a certain pair of parameters, and provides an indication on motor supplier, it lacks the ability to provide information on what the other parameters could be, or to allow searching for more than two parameters at once.

For the blank regions on the logarithmic plots, the further away from the populated regions the higher the likelihood that it is probably unlikely that an actuator could be found or designed and built to fulfill those parameters without being novel in nature. A potential example of what this could be, looking at the plots of torque vs power and torque vs weight, to find a motor on the top left of both of these plots simultaneously, i.e. to increase torque without increasing required power or weight of the motor, due to the torque on a coil equation (1) above, we cannot increase the number of coils or the area of the coils as that would increase weight, and we cannot increase the current as that will increase the power, hence it would require a stronger magnetic field. Considering a permanent magnet direct current motor, we cannot make the magnet bigger as that would increase the weight, and as such we would have to increase the magnetic field strength of the permanent magnet by finding a new material which is better than what is currently used. A novel solution would be the discovery and implementation of a high temperature superconductor that could be used for the permanent magnet.

5.2 Example application

This method of using these Ashby charts from a database as a design tool for the selection of an actuator, is applicable to any situation in which an actuator is required and not just for the field of biorobotics.

The significance of the utilization of the Ashby charts is that in the above example application, the utilization of the Ashby charts has allowed the reduction of the proportion of motors that the user needs to search down to 12.45% from the entirety of the database hence reducing search time. In addition, the resulting motor selection using the Ashby charts is more fit for the purpose based on the initial search criteria with torque and speed being as required with the power required being lower than the previously selected option. This is of significant importance, as shown by Hanna (2022) [20], as a slight improvement of motor selection has a substantial flow on effect for the rest of system design.

In this example, from the first figure alone we were able to eliminate most of the motor manufacturers from being suitable options, and the other plots didn't provide any additional insight, (besides for figures 14 and 15 where the lack of datapoints within the convex hull of the MOOG brushless motor within the bounded region shows that the database does not include a motor that is suitable for that manufacturer) however, there could be search parameters where only by considering multiple plots can the solution space be thoroughly filtered to provide a beneficial use of the plots. One other use of the method above, is that if no suitable manufacturers are found, the user can visually see which design parameter might need to be adjusted to include a solution. It also gives insight into which parameters might not be viable to change due to being an order of magnitude away from a datapoint.

6. FUTURE WORK

Further work that can be done includes recreating the Ashby charts with a different segregation parameter to depict groupings based on entities other than manufacturer. An entity that is anticipated to be of significant usefulness that has not been considered in this study is cost. One difficulty in creating such charts based on cost is that as it is a non-discrete parameter, significant consideration as to how the cost regions are defined is needed to allow widespread usefulness of the plots. Also, as cost is a volatile and non-constant parameter, creating charts with the underlying parameter as cost, is likely to be quickly made obsolete and so this needs to be solved first.

7. CONCLUSION

The Ashby charts presented in this paper can be used as a tool allowing designers of biorobotics to effectively narrow down actuators for their use cases. They make the process more efficient and provide direction on which manufacturers to consider or if a redesign is required.

ACKNOWLEDGEMENTS

This research is supported by an Australian Government Research Training Program Scholarship.

REFERENCES

[1] Nassour J., Hamker F.H., Cheng G., High performance perpendicularly enfolded textile actuators for soft wearable robots: design and realisation, IEEE Transactions on medical robotics and bionics, 2020; 2(3): pp 309-319

[2] T. Poliero et al., "Soft wearable device for lower limb assistance: Assessment of an optimized energy efficient actuation prototype," in Proc. IEEE Int. Conf. Soft Robot., Livorno, Italy, Apr. 2018, pp. 559–564.

[3] B. T. Quinlivan et al., "Assistance magnitude versus metabolic cost reductions for a tethered multiarticular soft exosuit," Sci. Robot., 2017, vol. 2, no. 2

[4] C. J. Nycz, T. Bützer, O. Lambercy, J. Arata, G. S. Fischer, and R. Gassert, "Design and characterization of a lightweight and fully portable remote actuation system for use with a hand exoskeleton," IEEE Robot. Autom. Lett., 2016, vol. 1, no. 2, pp. 976–983.

[5] K. Schmidt et al., "The myosuit: Bi-articular anti-gravity exosuit that reduces hip extensor activity in sitting transfers," Front. Neurorobot., vol. 11, p. 57, Oct. 2017.

[6] C. M. Best, J. P. Wilson, and M. D. Killpack, "Control of a pneumatically actuated, fully inflatable, fabric-based, humanoid robot," in Proc. IEEE-RAS 15th Int. Conf. Hum. Robots, Seoul, South Korea, Nov. 2015, pp. 1133–1140.

[7] H. K. Yap et al., "A fully fabric-based bidirectional soft robotic glove for assistance and rehabilitation of hand impaired patients," IEEE Robot. Autom. Lett., vol. 2, no. 3, pp. 1383–1390, Jul. 2017.

[8] X. Liang, H. Cheong, Y. Sun, J. Guo, C. K. Chui, and C. Yeow, "Design, characterization, and implementation of a two-DOF fabric-based soft robotic arm," IEEE Robot. Autom. Lett., vol. 3, no. 3, pp. 2702–2709, Jul. 2018.

[9] L. Cappello et al., "Exploiting textile mechanical anisotropy for fabric based pneumatic actuators," Soft Robot., vol. 5, no. 5, pp. 662–674, Oct. 2018.

[10] J. Bae et al., "A lightweight and efficient portable soft exosuit for paretic ankle assistance in walking after stroke," in Proc. IEEE Int. Conf. Robot. Autom., Brisbane, QLD, Australia, May 2018, pp. 2820–2827

[11] Prassler E., Advances in human-robot interaction, STAR, 2004; 14: pp23-34

[12] Sarkisian S.V., Ishmael M.K., Hunt G.R, Lenzi T., Design development and validation of a self-aligning mechanism for high torque powered knee exoskeletons, IEEE transactions on medical robotics and bionics, 2020; 2(2): pp 248-259

[13] M. A. Ergin and V. Patoglu, "A self-adjusting knee exoskeleton for robot-assisted treatment of knee injuries," in Proc. IEEE Int. Conf. Intell. Robot. Syst., 2011, pp. 4917–4922.

[14] L. M. Mooney, E. J. Rouse, and H. M. Herr, "Autonomous exoskeleton reduces metabolic cost of human walking while carrying a load," J. Neuroeng. Rehabil., vol. 11, no. 1, p. 80, 2014.

[15] T. Lenzi, D. Zanotto, P. Stegall, M. C. Carrozza, and S. K. Agrawal, "Reducing muscle effort in walking through powered exoskeletons," in Proc. Annu. Int. Conf. IEEE Eng. Med. Biol. Soc. (EMBS), 2012, pp. 3926–3929.

[16] S. Lefmann, R. Russo, and S. Hillier, “The effectiveness of robotic assisted gait training for paediatric gait disorders: Systematic review,” J. Neuroeng. Rehabil., vol. 14, no. 1, pp. 1–10, 2017.

[17] L. Saccares, I. Sarakoglou, and N. G. Tsagarakis, “it-Knee: An exoskeleton with ideal torque transmission interface for ergonomic power augmentation,” in Proc. IEEE Int. Conf. Intell. Robot. Syst., 2016, pp. 780–786.

[18] H. Kazerooni, “Exoskeletons for human power augmentation,” in Proc. IEEE/RSJ Int. Conf. Intell. Robot. Syst., Edmonton, AB, Canada, 2005, pp. 3459–3464.

[19] S. Kim, M. A. Nussbaum, M. I. M. Esfahani, M. M. Alemi, S. Alabdulkarim, and E. Rashedi, “Assessing the influence of a passive, upper extremity exoskeletal vest for tasks requiring arm elevation: Part I—‘Expected’ effects on discomfort, shoulder muscle activity, and work task performance,” Appl. Ergon., vol. 70, pp. 315–322, Sep. 2018.

[20] Hanna P., Carmichael M., & Clemon L., "Benefit of Optimal Actuator Selection – A Comparative Study" Proceedings of the ASME 2022 International Mechanical Engineering Congress and Exposition. Volume 4: Biomedical and Biotechnology; Design, Systems, and Complexity. Columbus, Ohio, USA, October 30-November 3, 2022.

[21] Birglen, L. and Gosselin, C.M., 2004. Kinetostatic analysis of underactuated fingers. IEEE Transactions on Robotics and Automation, 20(2), pp.211-221.

[22] Birglen, L. and Gosselin, C.M., 2003, September. On the force capability of underactuated fingers. In 2003 IEEE International Conference on Robotics and Automation (Cat. No. 03CH37422) (Vol. 1, pp. 1139-1145). IEEE.

[23] Al Al, A.Y.D., Bachtiar, A. and Harinita, D., 2019. An angle speed and thrust relationship of the quadcopter rotor. Indonesian Journal of Electrical Engineering and Computer Science, 13(2), pp.469-474

[24] Patterson, M.D. and Borer, N.K., 2017. Approach considerations in aircraft with high-lift propeller systems. In 17th AIAA Aviation Technology, Integration, and Operations Conference (p. 3782).

[25] Patterson, M.D., Borer, N.K. and German, B., 2016. A simple method for high-lift propeller conceptual design. In 54th AIAA Aerospace Sciences Meeting (p. 0770).

[26] Umar, C.M.I.C. and Zulkafli, M.F., 2021. Distance and Rotational Speed Analysis of Coaxial Rotors for UTHM C-Drone. Progress in Aerospace and Aviation Technology, 1(1), pp.46-55.

[27] Al, A., Dewi, A.Y. and Hidayat, T., 2018. The lifting force relationship of a BLDC motor rotor system to the blade rotation speed. In MATEC Web of Conferences (Vol. 215, p. 01013). EDP Sciences.

[28] McKay M.J., Baldwin J.N., Ferreira P., Simic M., Vanicek N., Burns J., Normative reference values for strength and flexibility of 1000 children and adults, American academy of neurology, 2017; 88: pp36-43

[29] Bohannon R.W., Reference values for extremity muscle strength obtained by handheld dynamometry from adults aged 20-79 years, Archives of physical medical rehabilitation, 1997; 78: pp26-32

[30] Gordon C.C., 1988 anthropometric survey of U.S. personnel: summary statistics interim report, Science and advanced technology directorate, 1989

[31] Dario P., Chatila R., Robotics research, STAR, 2005; 15: pp202-216

[32] Kagawa T., Nourma T., Kondo S., interlimb parallel-link powered orthosis (IPPO): compact wearable robotics with lateral weight bearing mechanisms for gait assistance, IEEE transactions on medical robotics and bionics, 2020; 2(3): pp300-308

[33] Tschiersky M., Heckman E.E.G., Brouwer D.M., Herder J.L., Gravity balancing flexure springs for an assistive elbow orthosis, IEEE transactions on medical robotics and bionics, 2019; 1(3): pp177-188

[34] Barjuei E.S., Ardakani M.M.G., Cladwell D.G., Sanguineti M., Ortiz J., Optimal selection of motors and transmissions in back support exoskeleton applications, IEEE transactions on medical robotics and bionics, 2020; 2(3): pp320-330

[35] Hanna P., Carmichael M., & Clemon L., "Development of an Organisational Framework for the Optimal and Efficient Selection of Actuators." Proceedings of the ASME 2021 International Mechanical Engineering Congress and Exposition. Volume 5: Biomedical and Biotechnology. Virtual, Online. November 1–5, 2021.